JOURNAL OF APPLIED ELECTROCHEMISTRY 17 (1987) 495–504

An oxygen sensor based on the semiconducting properties of $(U_{0.3}Y_{0.7})O_{2-x}$

S. P. S. BADWAL, F. T. CIACCHI

CSIRO, Division of Materials Science and Technology, Normanby Road, Clayton, Victoria 3168, Australia

Received 28 April 1986

Urania–yttria fluorite solid solutions with a U/Y ratio below 0.33/0.67 and having n-type conductivity are suggested as oxygen sensing materials. The electrical properties of one composition, $(U_{0.3}Y_{0.7})O_{2-x}$, have been studied in detail. The resistance of this composition follows a $(pO_2)^n$ relationship over an oxygen concentration range of 0.1 to 100% and shows long-term stability. The value of n decreases with increase in temperature (0.23 at 400° to 0.15 at 800° C), but is reproducible for a large number of specimens. A method for determining oxygen partial pressure in hot gases using these urania–yttria solid solutions as the sensing material is described.

1. Introduction

Several different types of oxygen sensor have been developed or are currently under development to fulfil the ever increasing demand for such devices [1–8]. The major uses are in car engine exhausts to control air/fuel ratio, in boiler flues for combustion control and in the chemical and metallurgical industries for process or quality control. Their usage has already led to significant reductions in the consumption of fuel and emission of toxic gases into the atmosphere. Three types of technologies currently attracting wider attention are: (i) zirconia Nernstian sensors, (ii) current mode operation zirconia cells, and (iii) sensors based on semiconducting properties of metal oxides. Zirconia Nernstian sensors with porous platinum electrodes do not provide accurate signals below about 600° C and are used mainly to monitor stoichiometric air–fuel ratios in car engine exhaust. With the use of metal oxide electrodes it may be possible to operate these sensors below about 400° C [1, 9, 10]. For the lean burn operation of the engine, where exhaust emission levels are low and fuel economy is high, the current mode sensor appears to be most promising at this stage and, consequently, considerable effort is being put into the research and development [4, 5] of this sensor. The current mode sensor is based on the oxygen pumping principle and consists of a single cell, or two zirconia cells joined together by a metal washer. The main advantage of this device is that, on application of an external voltage, it provides a current signal which is linearly proportional to the oxygen partial pressure whereas other types of sensors exhibit more complex relationships. The third category of sensor, and the subject of this paper, is based on the semiconducting properties of metal oxides. These sensors are serious contenders for other types of technologies. They are simple and conducive to miniaturization. The hybrid printed circuit technology with which such sensors can be manufactured lends itself to automation and mass production. Consequently, the sensor material, heater and the electrical connections can all be printed on a single substrate.

The principle of operation of the semiconducting oxygen sensor is that the resistance of a non-stoichiometric oxide can be represented by an expression of the form

$$R_0 \propto \exp(E/RT)(pO_2)^n \qquad (1)$$

where R_0 is the resistance of the metal oxide in an oxygen partial pressure of pO_2, E is the activation energy for conduction, R is the gas constant and T is the temperature (in K). The sign and value of n varies according to the defect chemistry of the metal oxide. Amongst metal oxide semiconductors, titania is by far the most

0021–891X/87 $03.00 + .12

widely studied material [2, 11]. The titania sensor, like the Nernstian oxygen sensor with porous platinum electrodes, is suitable only for monitoring the air/fuel ratio near stoichiometry. In this paper another system has been investigated with a view to develop a semiconducting oxygen sensor for lean burn applications (boilers, engine exhaust, etc.).

Uranium oxide forms fluorite solid solutions with yttria, scandia and several rare earth oxides over a wide composition range [12–15]. These solid solutions are structurally stable over wide ranges of temperature and oxygen partial pressure. They generally undergo fast oxidation–reduction reactions at the gas–solid interface because of the variable valence of uranium. In these solid solutions the average oxidation state of uranium increases with decrease in the U/M ratio (where M = scandia, yttria or rare earth metal). Theoretically when the U/M ratio decreases below 0.33/0.67 and the lattice still has the fluorite structure, uranium exists in its maximum oxidation state (6+) and the lattice is anion deficient [14, 16]. Wilson *et al.* [17], in the case of the U–La–O system, have reported that the conduction mode changes from p- to n-type when the U/La ratio decreases below 0.33/0.67. This also appears to be the case for the U–Y–O system (see below). The value of n (Equation 1) for U/Y ratios above 0.33/0.67 is less than 0.1 for oxygen concentrations between 15 and 1% (typical lean burn region) and hence the relative change in resistance of the metal oxide with oxygen partial pressure is also low. However, for the narrow anion deficient composition range, between U/Y ratios of 0.33/0.67 to the stability limit of the fluorite structure, the value of n (see below) is comparable with that for titania [18] and this composition range is the subject of the present study. This paper reports the electrical characteristics of one composition from this urania–yttria fluorite solid solution range and laboratory trials of sensors based on this material.

2. Experimental procedures

A powder of composition $(U_{0.3}Y_{0.7})O_{2-x}$ was prepared by co-precipitation of the mixed hydroxides with aqueous ammonia from a solution containing the required proportions of uranyl and yttrium nitrates, followed by drying and calcination in air at 700° C. Room-temperature X-ray powder diffraction confirmed the presence of a single fluorite phase. The reacted powder was pressed into disc or bar shapes and sintered either at 1300 or 1400° C for 15 h in air. Rectangular specimens with the dimensions l = 6–10 mm, h = 3–5 mm, w = 3–5 mm were sliced from sintered discs or bars for determining electrical characteristics of $(U_{0.3}Y_{0.7})O_{2-x}$. Alternatively, the calcined powder was painted as a paste in triethylene glycol on high-density alumina substrates followed by heat treatment in the 600–800° C temperature range. In addition to the co-precipitation technique, some specimens were also prepared by sintering the pressed discs of premixed U_3O_8 and Y_2O_3 powders.

The resistance of several such specimens was determined as a function of temperature and oxygen partial pressure. Both two- and four-probe d.c. techniques were used for carrying out resistance measurements. The two ends of the specimens were platinized with Engelhard platinum paste 6082 followed by firing at 600–700° C to burn off the organics. Platinum wire (diameter 0.25 mm) was wrapped around each platinized end and, in addition, another two platinum wire contacts, as shown in Fig. 1, were made for measuring the voltage drop in the four-probe arrangement. For two-probe measurements, only the end contacts were used for passing current as well as measuring the voltage drop. The current through the outer probes was passed by a Keithley constant current source model 225 and the potential across the same or inner probes was measured with a Hewlett Packard 3472 digital multimeter (input impedance $10^{10}\,\Omega$).

In order to determine the resistance–temperature relationship at various oxygen partial pressures, the specimens were initially heated to a temperature between 650 and 800° C in air and the data recorded during several heating and cooling cycles at about 25° C temperature intervals. The gas composition was changed only at the highest temperature of measurement and sufficient time was allowed for specimens to come to equilibrium with the new gas atmosphere. To establish a relationship between the

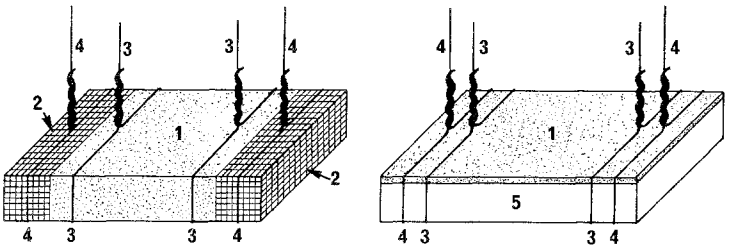

Fig. 1. Schematics of two specimen assemblies. 1, $(U_{0.3}Y_{0.7})O_{2-x}$; 2, platinum paste; 3, platinum potential probes for the four-probe arrangement, 4, current probes; 5, alumina substrate.

resistance and the oxygen partial pressure, the cell was taken at least 50° C above the highest measurement temperature, left for 15–20 h and cooled to the desired temperature. The resistance was then determined in various gas atmospheres over an oxygen partial pressure range of $1–10^{-3}$ atm. These measurements were made at one or more temperatures on a number of specimens between 400 and 800° C.

For the determination of the Seebeck coefficient a temperature gradient across the two ends of the specimen (about 1 cm long) was established by positioning it away from the constant temperature zone of the furnace. Measurements were made at several temperatures with a temperature difference typically in the range 5–10° C. The temperature at each end of the specimen was determined by making thermocouple contact to platinum foils pressed directly against each end.

Some preliminary response rate measurements were also made in order to determine the resistance–time response of $(U_{0.3}Y_{0.7})O_{2-x}$ slabs to oxygen partial pressure changes. Two techniques were used for this purpose. The first involved evacuating the specimen chamber followed by switching the atmosphere to air with a fast solenoid valve. In the second technique a simple step change in oxygen concentration was made by alternatively changing the gas composition between air and 1% O_2 in N_2. The change in the voltage signal as a function of time, for a constant current flowing through the specimen, was either recorded on a chart recorder or with a programmable Keithley model 192 digital multimeter. The details of the response rate rigs will be published elsewhere [19].

3. Electrical characteristics

Since the actual values of resistivities are irrelevant to the measurement of oxygen concentra-

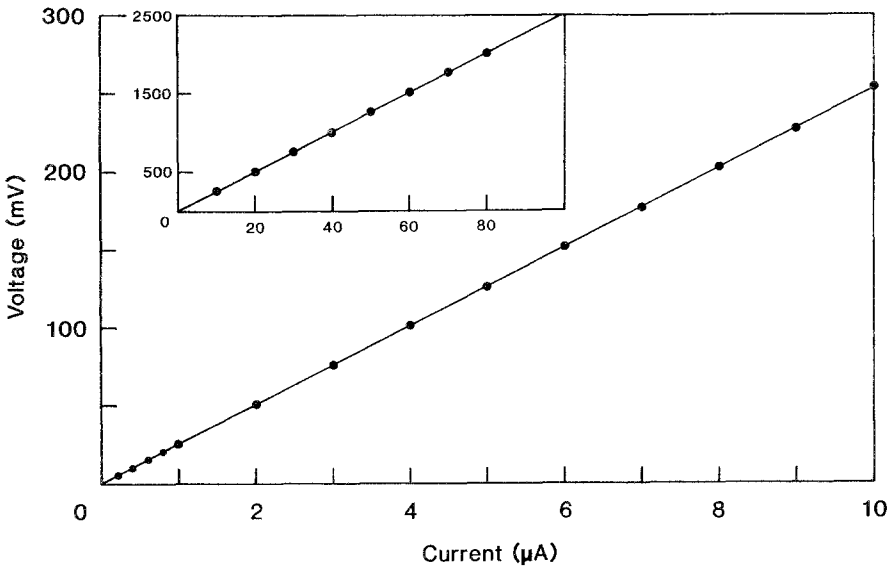

Fig. 2. Current–voltage plot for a $(U_{0.3}Y_{0.7})O_{2-x}$ specimen from the two-probe assembly.

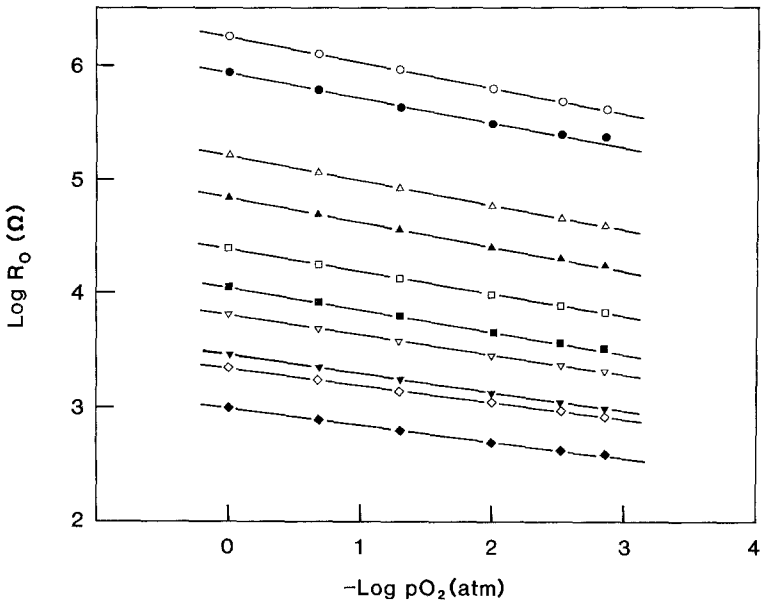

Fig. 3. Plots of log(specimen resistance) versus log(pO_2) at various temperatures for two specimens. ●○, 400° C, ▲△, 500° C; ■□, 600° C; ▼▽, 700° C; ◆◇, 800° C. Open symbols, sample A; closed symbols, sample F.

tion, no attempt has been made to apply a correction to resistances. The current–voltage plot for a two-probe assembly is shown in Fig. 2. The relationship between current and voltage is linear over a wide range of current indicating that the contact between platinum and $(U_{0.3}Y_{0.7})O_{2-x}$ is ohmic. Fig. 3 shows plots of log(resistance) versus log pO_2 for two slab-type specimens. The resistance (R_0) values reported are those determined by the two-probe technique. For all the specimens studied, the relationship between log R_0 versus log pO_2 was linear over the oxygen partial pressure range of 1.0–0.003 atm. The values of n for several specimens determined from linear least squares fit of the data at various temperatures are given in Table 1. The value of n at a constant temperature is independent of the method of preparation of the urania–yttria composition (co-precipitation or by mixing uranium and yttrium oxides), the calcination and sintering temperatures, the cell geometry and the technique (two- or four-probe) used to measure the resistance.

Fig. 4 shows plots of electrical resistance versus reciprocal temperature in various oxygen partial pressures for one specimen. The values of activation energy for conduction are given in Table 2. A similar value in an oxygen partial pressure of 0.21 atm was reported earlier for $(U_{0.3}Y_{0.7})O_{2-x}$ [20]. The activation energy decreases slightly with decrease in the oxygen partial pressure.

The values of the Seebeck coefficient at 600° C is $-365 \pm 10\,\mu V\,°\,C^{-1}$. The absolute Seebeck coefficient of the oxide can be determined by applying a correction for the Seebeck coefficient of platinum which is $-11.7\,\mu V\,°\,C^{-1}$ at 600° C

Table 1. Values of n *over the oxygen partial pressure range of 1.0–0.003 atm for* $(U_{0.3}Y_{0.7})O_{2-x}$

Specimen	*Type*	n(±0.002)				
		400° C	*500° C*	*600° C*	*700° C*	*800° C*
A	Slab	0.227	0.217	0.200	0.177	0.147
B	Slab	0.227	0.219	0.200	–	–
C	Painted	–	–	0.200	–	–
D	Slab	–	0.217	0.198	–	–
E	Painted	–	–	0.201	–	–
F	Slab	0.227	0.217	0.197	0.175	0.148

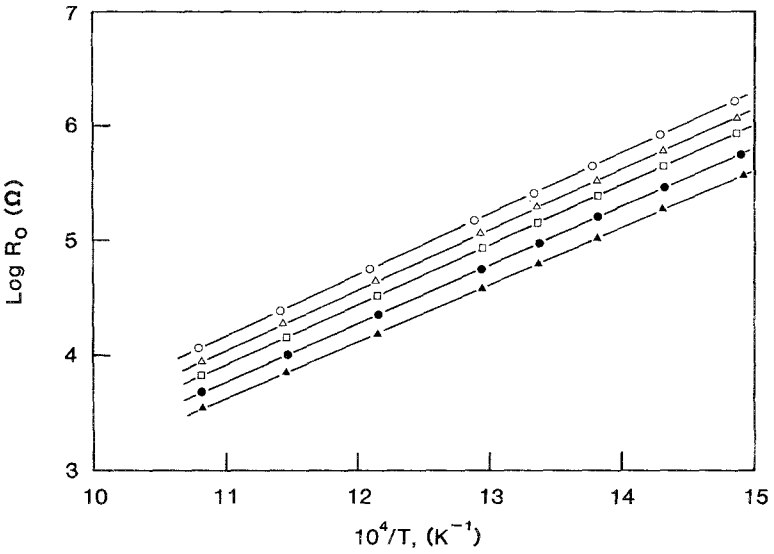

Fig. 4. Arrhenius plots for the two-probe resistance of $(U_{0.3}Y_{0.7})O_{2-x}$ in various oxygen partial pressures. Values of pO_2 (atm): ○, 1.0; △, 0.2095; □, 5.08×10^{-2}; ●, 1.01×10^{-2}; ▲, 1.4×10^{-3}.

[21]. The sign of the Seebeck coefficient clearly indicates that the $(U_{0.3}Y_{0.7})O_{2-x}$ composition is an n-type conductor. Similar measurements on specimens for which the U/Y ratio was greater than 0.4/0.6 showed these materials to be p-type conductors.

4. Suitability of $(U_{0.3}Y_{0.7})O_{2-x}$ as an oxygen sensor

4.1. *Response to changes in* pO_2

In general, the resistance response of an oxide semiconductor sensor to oxygen partial pressure changes increases with increase in the value of n (Equation 1). The value of n reported for other metal oxides such as SnO_2, CoO, ZnO and TiO_2 [2, 3] lies between 0.1 and 0.25. For $(U_{0.3}Y_{0.7})O_{2-x}$, n varies between 0.23 (at 400° C) and 0.15 (at 800° C).

The theoretical response of the Nernstian sensor relative to air as the reference atmosphere is given by

$$E(\text{mV}) = 0.0496T \log (0.2095/pO_2) \quad (2)$$

For the semiconducting sensor, with air as the calibration gas ($pO_2 = 0.2095$ atm), the unknown oxygen partial pressure p^uO_2 is given by

$$p^uO_2(\text{atm}) = 0.2095(R_0/R_1)^{1/n} \quad (3)$$

For comparison with the Nernst sensor this equation needs to be converted to the form

$$E(\text{mV}) = (p^uO_2/0.2095)^n IR_1 \quad (4)$$

where R_0 is the resistance in an atmosphere whose oxygen partial pressure is to be measured, R_1 is the resistance of the sensor in air and I is a constant current flowing through the sensor.

Fig. 5 compares the voltage response of $(U_{0.3}Y_{0.7})O_{2-x}$ and Nernstian sensors as a function of oxygen partial pressure. As shown in this figure, the sensitivity of the semiconductor

Table 2. Activation energy for conduction in various oxygen partial pressures for $(U_{0.3}Y_{0.7})O_{2-x}$ over the temperature range 400–650° C

Specimen	E ± *1 (kJ mol^{-1})*				
	1.0 atm	*0.2095 atm*	*0.0508 atm*	*0.0101 atm*	*0.0014 atm*
A	101.8	99.8	99.0	97.7	95.2
B	101.3	–	–	–	–
C	102.3	–	–	–	–

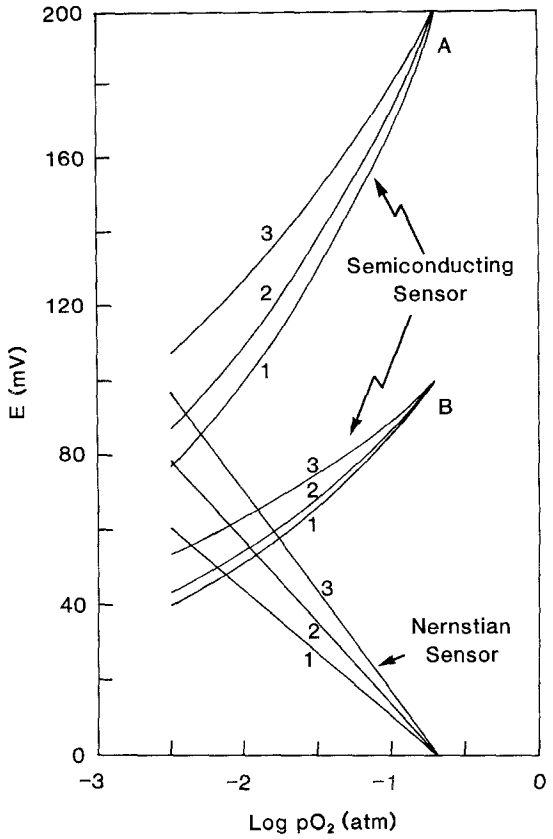

Fig. 5. Voltage response of Nernstian and $(U_{0.3}Y_{0.7})O_{2-x}$ (IR_1 = 200 mV for A and 100 mV for B) sensors over oxygen concentration range of 0.3–21%. 1, 400° C; 2, 600° C; 3, 800° C.

sensor may be varied by changing the value of product IR_1 whereas that of the Nernstian sensor is fixed.

4.2. *Temperature dependence of* n

Although the value of n is reproducible at a given temperature for a large number of specimens, it nevertheless varies with temperature. This could be a major drawback as the process temperature in industrial environments may fluctuate considerably with time. Use of an approximate value of n to calculate an unknown oxygen partial pressure will introduce unnecessary errors. In order to find a simple solution to this problem, a polynomial fit was tried to the data in Table 1. As shown in Table 3 the agreement between the calculated (from the coefficients of a third degree polynomial) and

Table 3. Comparison of experimental values of n *with those determined from polynomial regression*

T (±1) (° C)	n *(experimental)*	n *(polynomial regression)*
400	0.227	0.22703
500	0.217	0.21689
600	0.200	0.20017
700	0.177	0.17688
800	0.147	0.14703

measured values is excellent. The advantage of such a good fit is that it not only eliminates the need to determine n experimentally at several temperatures, but now the oxygen partial pressure can be determined at any process temperature from the known value of n and the calibration constant.

4.3. *Response time*

The response time of the $(U_{0.3}Y_{0.7})O_{2-x}$ (measured for slab type specimens) is slower compared with the Nernstian sensor. Typical response times at 600° C were in the 5 to 25 s range. These are at least an order of magnitude higher than those measured for the Nernstian sensor under identical conditions [19]. We believe that this is so because the sensors were in the form of slabs with small area for gas–solid reaction and longer diffusion paths. Since sensors may also be prepared in thick film form, as has been mentioned earlier, it seems likely that the response time will improve.

4.4. *Temperature coefficient*

The temperature coefficient of the sensor is essentially determined by the resistance–temperature relationship. For $(U_{0.3}Y_{0.7})O_{2-x}$ the activation energy for conduction is 102 kJ mol^{-1}, considerably lower than the 155 kJ mol^{-1} reported for titania [2]. The temperature coefficient of resistance is 2.5% ° C^{-1} at 400° C and 1.5% ° C^{-1} at 600° C for $(U_{0.3}Y_{0.7})O_{2-x}$. These values, nevertheless, are much larger than those of the Nernstian sensor which, for example, has the temperature coefficient of only 0.15% ° C^{-1} at 600° C. It is therefore vital to measure the temperature of the semiconductor sensing material accurately. In environments where large temperature

fluctuations can occur over a very short period the sensor may not be suitable unless it is of very small size and is equipped with an external heater.

4.5. *Measurement technique*

From the two- and four-probe measurements made on a large number of specimens, a two-probe assembly appears to be adequate for most of the applications. In environments where the contact resistance at the metal/$(U_{0.3}Y_{0.7})O_{2-x}$ interface is likely to change due to thermal or mechanical shocks or due to reaction between the contact material and hot gases, a four-probe assembly is more suitable.

4.6. *Calibration requirements*

One of the disadvantages of the semiconducting sensors is that if used to measure absolute oxygen concentration, they require calibration at the time of installation. The value of the calibration constant may change with time especially in industrial environments. The frequency with which the sensor needs to be recalibrated will have significant bearing on its suitability as a practical device. In a plant trial conducted at 700° C on a slab-type specimen in the boiler flue of a gas-fired industrial boiler, the resistance of the sensor in air (the calibration constant) measured by a two-probe technique drifted by 3% over a period of 4 months. This corresponds to about 16% error in the oxygen partial pressure measurements for the calibration gas. However, most of this error (12.5%) occurred in the first 6 weeks of operation.

5. Sensor tests

Following the initial work on characterization of electrical properties of $(U_{0.3}Y_{0.7})O_{2-x}$ composition, three sensors were prepared for laboratory tests. One of these was prepared by painting a paste of $(U_{0.3}Y_{0.7})O_{2-x}$ in triethylene glycol on an alumina substrate, while the other two were the normal slab-type specimens used for measurement of electrical properties. For measuring resistance, only two electrical contacts were made to the sensor material.

With one slab-type and the painted sensor, oxygen concentration measurements were made at a number of fixed temperatures between 600 and 450° C. The procedure involved heating the sensor to 600° C in air at the start of the test and recording the resistance. The gas composition around the sensor and/or the temperature of the sensor were then changed and the oxygen partial pressure was calculated from the measured resistance and from the known values of n and the calibration constant (the resistance of the sensor in air at 600° C) using Equation 3. Values for the calibration constant (R_1) at temperatures other than 600° C were obtained from its value at 600° C and the activation energy for conduction in air. The value of n at various temperatures was computed from the coefficients of the polynomial described in the previous section. Table 4 shows excellent agreement between the measured and known oxygen concentrations.

The third sensor was subjected to exhaustive oxygen partial pressure and temperature cycling tests. A block diagram of the microprocessor-based equipment used for these tests is shown in Fig. 6. At the beginning of the experiment the sensor was slowly heated to 600° C in air, and R_1 was determined at this temperature and stored in

Table 4. Comparison between calculated and known values of oxygen concentrations for two sensors

T (° C)	*Known oxygen concentration (%)*	*Calculated oxygen concentration*	
		Sensor 1 (slab)	*Sensor 2 (painted)*
600	1.01	–	1.05
600	5.08	–	5.15
600	20.95	–	21.13
602	100.0	100.3	–
563	20.95	20.5	–
563	5.08	4.93	–
563	1.01	1.03	–
533	1.01	1.01	–
533	5.08	4.93	
534	20.95	20.7	
452	20.95	21.8	
452	1.01	1.09	
499	1.01	0.95	
499	5.08	4.97	
499	20.95	21.0	
499	100.0	100.2	

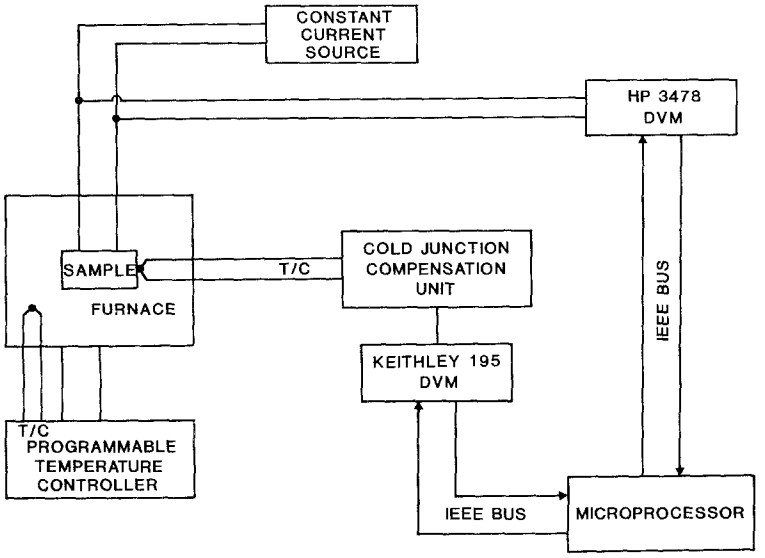

Fig. 6. A block diagram of the computer-controlled sensor test equipment.

the microprocessor unit along with the value of n (at 600° C) to determine oxygen partial pressure using Equation 3. In the first stage of the experiment the temperature was kept constant (to within ± 1° C) and the sensor was subjected to atmospheres of a variety of oxygen partial pressures (between 1 and 10^{-3} atm) with gas changes being made at intervals of 12 to 24 h. The resistance, R_0, of the sensor was monitored continuously over a period of several days with the equipment shown in Fig. 6. Over this period, without recalibration, the errors in oxygen partial pressure measurements increased slowly to about 3%.

In the second stage of the experiment, the sensor after redetermination of the calibration constant (resistance in air at 600° C) was first cycled between 600° and 300° C at a heating and a cooling rate of 0.5° C min^{-1} for 25 days (one heating–cooling cycle per day including 4 h dwell time at 600° C), and then between 600° C and room temperature at a heating and a cooling rate of 2.0° C min^{-1} (except where thermal inertia of the furnace dictated a slower cooling rate) for 19 days. Oxygen partial pressure changes, similar to those in the first stage of this experiment, were made only when the temperature was at the 600° C part of thermal cycle. The

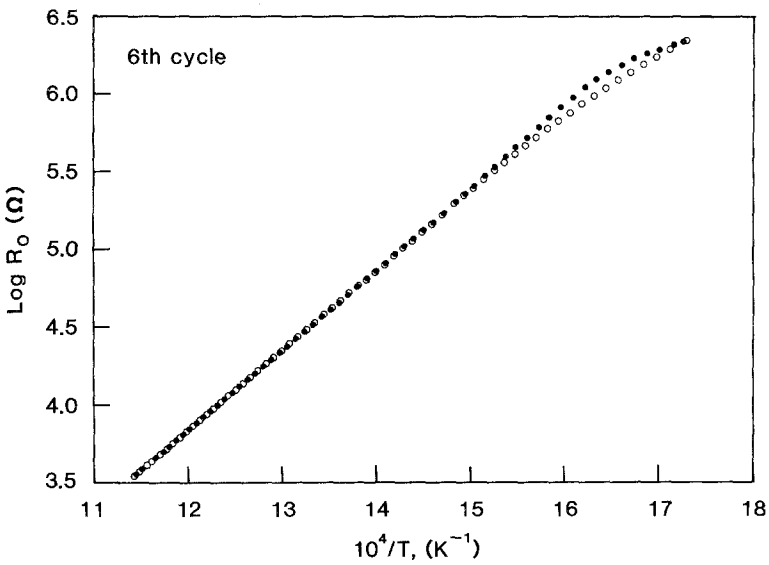

Fig. 7. Arrhenius plot of the sensor resistance in air for the 6th thermal cycle. ●, heating cycle; ○, cooling cycle.

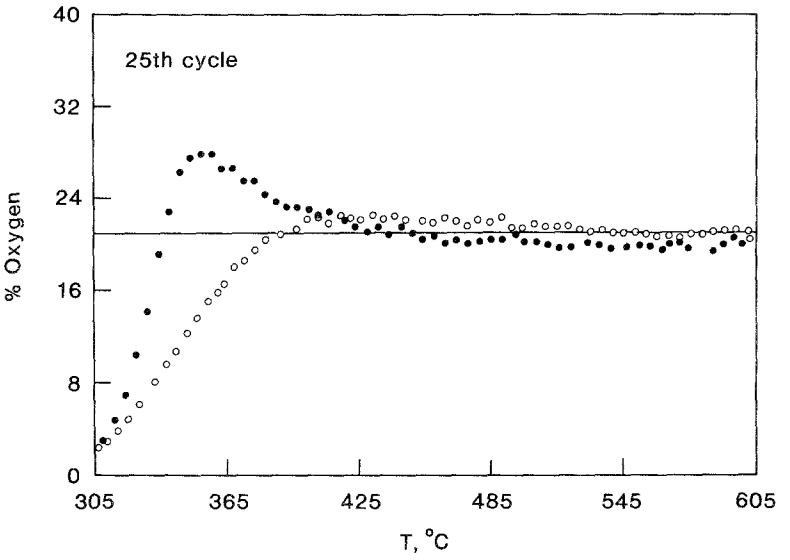

Fig. 8. A plot of the calculated oxygen partial pressure versus temperature for the 25th heating (●) and cooling (○) cycles. The solid line represents the actual oxygen concentration around the sensor.

procedure for calculating the oxygen partial pressure involved:

(i) continuously measuring the temperature and resistance (with a time lag of 3–4 s);

(ii) computing a new value for R_1 at the temperature of the sensor from the previously stored value at 600° C and the value of the activation energy for conduction in air (Table 2);

(iii) computation of the value of n at the temperature of the sensor from the previously determined polynomial; and

(iv) determining the oxygen partial pressure using Equation 3 and the measured resistance, R_0.

Fig. 7 shows a typical Arrhenius plot of the sensor resistance and in Fig. 8 calculated oxygen partial pressure is plotted against temperature for a typical cooling and a heating cycle. Over the 44 thermal cycles of the second stage of the test, errors at the static temperature (600° C) of the thermal cycle were less than 5%, as shown in Fig. 9. Larger errors (up to 10%) were observed

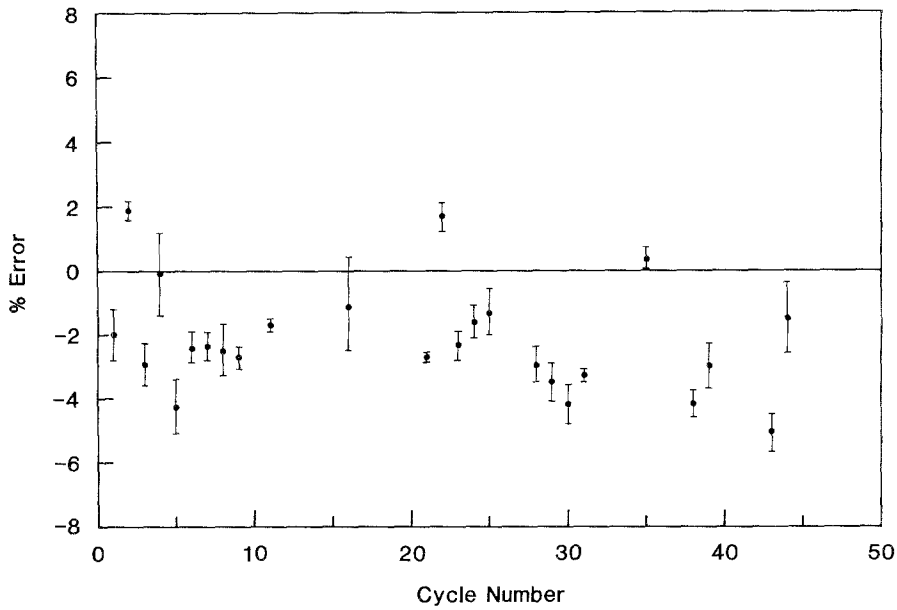

Fig. 9. A plot of the percentage error in oxygen concentration measurements versus cycle number at 600° C. Each cycle corresponds to 24 h.

during the heating and cooling, but these are at least in part due to the time-lag between measurement of temperature and the resistance introduced by the microprocessor program. Finally, marked hysteresis in the sensor resistance (Fig. 7) was observed below 390° C. This is also reflected in the calculation of the oxygen partial pressure (Fig. 8). The reason for this behaviour has not been investigated so far. The sign of the error at 600° C (Fig. 9) is consistent with a slight increase in the value of the calibration constant (the resistance in air) with time. It is most likely that this increase is associated with an increase in the contact resistance at the platinum/$(U_{0.3}Y_{0.7})O_{2-x}$ interface rather than the bulk resistance of the sensor. Use of the four-probe technique should considerably reduce or eliminate this problem.

6. Conclusions

The semiconductor oxygen sensor based on $(U_{0.3}Y_{0.7})O_{2-x}$ shows considerable promise and is ideally suited for lean burn applications. The success or failure of the sensor, apart from its electrical, chemical and mechanical stability in industrial environments, also depends upon whether or not adherent thick films of the sensor material on a substrate can be commercially produced. The latter is important for fast response rates and mass production of the sensors. Industrial trials of the sensor in the form of a slab with two electrical contacts are currently being conducted.

Acknowledgements

The authors are thankful to W. G. Garrett for performing vacuum response rate tests, B. Terrell for co-precipitation and Novatech Controls Pty Ltd for conducting industrial trials of the sensor. The manuscript was kindly reviewed by W. G. Garrett.

References

[1] S. P. S. Badwal, M. J. Bannister and W. G. Garrett, *J. Phys. E: Sci. Instrum.*, to be published.
[2] D. E. Williams and P. McGeehin, 'Electrochemistry', Vol. 9, The Royal Society of Chemistry, London (1984) p. 246.
[3] T. Seiyama, K. Fueki, J. Shiokawa and S. Suzuki (eds), 'Chemical Sensors', Analytical Chemistry Symposia Series, Vol. 17, Proceedings of the International Meeting on Chemical Sensors, Fakuoka, Japan, 19–22 September 1983, Elsevier, Amsterdam (1983).
[4] 'SAE Technical Paper Series', Passenger Car Meeting, Dearborn, Michigan, 1–4 October 1984.
[5] 'SAE Technical Paper Series', International Congress and Exposition, Detroit, Michigan, 25 February–1 March 1985 (SAE, Warrendale, Pennsylvania).
[6] R. M. A. Kocache, J. Swan and D. F. Holman, *J. Phys. E: Sci. Instrum.* **17** (1984) 228.
[7] G. Valasco and J-Ph. Schnell, *J. Phys. E: Sci. Instrum.* **16** (1983) 973.
[8] O. de Pous, *Fachberichte Sprechsaal* **117** (1984) 228.
[9] S. P. S. Badwal, M. J. Bannister and W. G. Garrett, in 'Advances in Ceramics', Vol. 12 (edited by M. Ruhle, N. Claussen and A. H. Heuer), The Amer. Ceram. Soc. Inc., Columbus, Ohio (1984) p. 598.
[10] S. P. S. Badwal and F. T. Ciacchi, *J. Appl. Electrochem.* **16** (1986) 28.
[11] J. L. Pfeifer, T. A. Libsch and H. P. Wertheimer, SAE Paper No. 840142, SAE Technical Paper Series, Passenger Car Meeting, Dearborn, Michigan, 1–4 October 1984.
[12] S. F. Bartram, E. F. Juenke and E. A. Aitken, *J. Amer. Ceram. Soc.* **47** (1964) 171.
[13] R. J. Beals and J. Handwerk, *ibid.* **48** (1965) 271.
[14] D. C. Hill, *ibid.* **45** (1962) 260.
[15] W. Trzebiatowski and P. Horyn, *Bull. De l'Academie Polonaise des Sciences* **XV** (1967) 191.
[16] E. A. Aitken and R. A. Joseph, *J. Phys. Chem.* **70** (1966) 1090.
[17] W. B. Wilson, C. A. Alexander and A. F. Gerds, *J. Inorg. Nucl. Chem.* **20** (1961) 242.
[18] S. P. S. Badwal, unpublished work.
[19] W. G. Garrett, CSIRO, Division of Materials Science, Internal Report, to be published.
[20] S. P. S. Badwal and D. J. M. Bevan, *J. Mater. Sci.* **14** (1979) 2353.
[21] N. Cusack and P. Kendall, *Proc. Roy. Soc. London* **72** (1958) 898.